



Scott, S. J., Greaves, P., Macquart, T., & Pirrera, A. (2022). Comparison of blade optimisation strategies for the IEA 15 MW reference turbine. *Journal of Physics: Conference Series*, 2265(3), [032029]. <https://doi.org/10.1088/1742-6596/2265/3/032029>

Publisher's PDF, also known as Version of record

License (if available):
CC BY

Link to published version (if available):
[10.1088/1742-6596/2265/3/032029](https://doi.org/10.1088/1742-6596/2265/3/032029)

[Link to publication record in Explore Bristol Research](#)
PDF-document

This is the final published version of the article (version of record). It first appeared online via IOP Publishing at <https://iopscience.iop.org/article/10.1088/1742-6596/2265/3/032029>. Please refer to any applicable terms of use of the publisher.

University of Bristol - Explore Bristol Research

General rights

This document is made available in accordance with publisher policies. Please cite only the published version using the reference above. Full terms of use are available: <http://www.bristol.ac.uk/red/research-policy/pure/user-guides/ebr-terms/>

PAPER • OPEN ACCESS

Comparison of blade optimisation strategies for the IEA 15MW reference turbine

To cite this article: Samuel Scott *et al* 2022 *J. Phys.: Conf. Ser.* **2265** 032029

View the [article online](#) for updates and enhancements.

You may also like

- [UK perspective research landscape for offshore renewable energy and its role in delivering Net Zero](#)
Deborah Greaves, Siya Jin, Puiwah Wong et al.
- [Wind farm optimization with multiple hub heights using gradient-based methods](#)
Andreas Wolf Ciavarra, Rafael Valotta Rodrigues, Katherine Dykes et al.
- [Modeling and analysis of the solar photovoltaic levelized cost of electricity \(LCoE\) - case study in Kupang](#)
Rusman Sinaga, Nonce F. Tuati, Marthen D.E. Beily et al.




ECS The Electrochemical Society
Advancing solid state & electrochemical science & technology

242nd ECS Meeting



Oct 9 – 13, 2022 • Atlanta, GA, US

Presenting more than 2,400 technical abstracts in 50 symposia

ECS Plenary Lecture featuring M. Stanley Whittingham,
Binghamton University
Nobel Laureate –
2019 Nobel Prize in Chemistry

 **Register now!**



Comparison of blade optimisation strategies for the IEA 15 MW reference turbine

Samuel Scott^{1,2}, Peter Greaves¹, Terence Macquart² & Alberto Pirrera²

¹Offshore Renewable Energy Catapult, Offshore House, Albert Street, Blyth, NE24 1LZ, UK.

²Bristol Composites Institute, University of Bristol, Queen's Building, University Walk, Bristol, BS8 1TR, UK.

E-mail: peter.greaves@ore.catapult.org.uk

Abstract. Reference wind turbine models are crucial for enabling the research community to advance technology and meet the challenges associated with upscaling. The IEA 15 MW is one such reference model, designed using NREL's WISDEM tool, which enables researchers to perform system-level analysis and optimisation. However, the authors have found the blade to be structurally infeasible when subject to aero-servo-elastic simulations and finite-element (FE) analyses. Given the shortcomings, this work aims to develop an updated blade model for the 15 MW turbine platform using the design tool **Aeroelastic Turbine Optimisation Methods (ATOM)**. Two optimisation processes, with a comprehensive suite of feasibility constraints, are applied: 1) a frozen-loads mass minimisation with fixed planform, and 2) an aero-servo-structural levelised cost of energy (LCoE) minimisation. Results show the frozen-loads optimised design results in a 0.93% increase in LCoE due to the mass penalty of attaining feasibility. In contrast, the aero-structural optimised design results in a 2.29% reduction in LCoE due to mass reductions and increased energy capture—highlighting the benefits of an integrated design process. FE shell analysis of the optimised blades indicates the strength predictions in **ATOM** are accurate and the main load-bearing spar caps are optimally utilised. Whilst an improvement on the baseline, buckling load factors do not satisfy the target values, indicating the lower fidelity checks in **ATOM** are non-conservative. The WindIO yaml files for these optimised designs are freely available online.

1 Introduction

Upscaling of wind turbines is an effective lever for reducing the levelised cost of energy (LCoE). However, in order for academic communities to contribute to the ensuing challenges, realistic reference models are needed that keep up with the rapid pace of technology development. A number of reference turbines have been developed over the years, including the NREL 5 MW [1], the DTU 10 MW [2], and the IEA 3.4 MW [3]. More recently, NREL and DTU developed and publicised a 15 MW reference wind turbine, as part of the IEA Wind Task 37 [4], sized in line with several recently announced multi-MW turbines (GE Haliade-X, Vestas V236-15MW and Siemens-Gamesa SG 14-222 DD). The 15 MW turbine was designed using NREL's WISDEM [5] tool, and all relevant data is published according to the [WindIO](#) ontology on [GitHub](#).



Content from this work may be used under the terms of the [Creative Commons Attribution 3.0 licence](#). Any further distribution of this work must maintain attribution to the author(s) and the title of the work, journal citation and DOI.

Various projects under the Wind Blades Research Hub (WBRH), a collaboration between the Offshore Renewable Energy (ORE) Catapult and the University of Bristol, are currently using the IEA 15 MW blade as a starting point—predominantly to investigate sustainable materials, aeroelastic stability, and additive manufacturing. However, through refined analyses of the baseline turbine, structural and aeroelastic stability issues have been identified. In particular, the original authors recommend a fictitiously high structural damping (3%), which is required for stable aero-servo-elastic simulations when using a modal reduction of the blades. Furthermore, the ultimate load envelopes—when applied to a finite element (FE) model of the blade—result in significant strength and buckling failures. Whilst small discrepancies between models and aeroelastic codes are common [6], using a baseline blade with significant failures has been deemed unsuitable for the intended projects.

Given the aforementioned pitfalls of the original design, this work's aim is to develop an updated blade model for the existing 15 MW turbine platform that is feasible and representative of the current state-of-the-art. Two optimisation processes of increasing complexity are employed for the task. The first, a 'frozen-loads' approach demonstrated by various authors [7]–[9], generates a mass-optimal internal blade structure given a fixed platform. The second is an integrated aero-structural optimisation that designs aerodynamic, structural, and operational parameters to minimise LCoE. Both methods are performed using the multi-disciplinary analysis and optimisation (MDAO) tool known as **ATOM** (**A**eroelastic **T**urbine **O**ptimisation **M**ethods) [9]–[11], co-developed under the WBRH. Finally, the structural feasibility of the optimised designs is assessed using FE shell analyses.

The methods used in this work are described in Section 2, followed by the analyses of the baseline 15 MW turbine in Section 3. Section 4 then presents the optimisation results, and lastly, the FE analyses are discussed in Section 5.

2 Methods

2.1 Load simulations

Two aero-servo-elastic simulations methods are employed in this work. The first is used for the baseline analysis and frozen-loads optimisation, and couples blade-element-momentum theory and a dynamic blade model based on modal reduction (15 blade modes) in a fixed-point iteration scheme. Dynamic control is provided by a simple PI controller with gain schedules found in the relevant ROSCO controller [12]. The first method employs a reduced set of IEC design load cases (DLCs) [13]—1.1, 1.3, 2.3, and 6.1—as these have been found to offer a good estimate of ultimate blade loads without excessive computational effort.

The second analysis method uses an aeroelastic piecewise linearised model of the rotor [14] for the aero-structural optimisation. A further reduced set of DLCs is used, consisting of 11, 600 s simulations from DLC 1.1 and 1.3. Whilst such a reduced set may not capture all extreme/fatigue loads, a compromise between accuracy and computational time is required. Note, both simulation methods assume a monopile foundation, with no wave loading present.

2.2 Optimisation

The optimisation problem formulations are now described. However, a number of features/modifications common to both processes are first explained. The nacelle, tower and foundations are assumed identical to the baseline. Conversely, the material properties used for the blade, defined in Table 1, are modified based on in-house data—in particular the strength values are more realistic. Blade structural damping is also set to 0.5%.

Several changes to the blade structural configuration are described as follows:

Table 1: Material properties used for optimisation.

Name	E11 (GPa)	E22 (GPa)	G12 (GPa)	ν_{12} (-)	ρ (kgm ⁻³)	Xt (MPa)	Xc (MPa)	Yt (MPa)	Yc (MPa)	S (MPa)
UD glass	43.2	12.6	4.42	0.29	1926	777	648	48.6	157	90.3
BIAX glass	13.4	13.4	12.1	0.53	1910	300	185	300	185	144
UD carbon	129.2	7.62	3.81	0.32	1548	1954	967	46.6	158	55
Foam	0.13	0.13	0.05	0.32	130	2.1	1.56	2.1	1.56	1.25

- (i) Shear webs are extended closer to the blade root and tip—to avoid stress concentrations.
- (ii) Spar caps contain UD glass and carbon layers, allowing the optimiser to control the ratio.
- (iii) Skins contain independent glass UD and BIAX layers, as opposed to TRIAX in the baseline.
- (iv) Sandwich core thickness may vary independently, depending on the optimisation.
- (v) Root bolt diameter is optimised. Whilst not modelled in the beam/aeroelastic model, root connection mass is considered in the cost model. A bolt stress constraint is applied, based on a scaling law from in-house data, which enables a realistic blade mass and root chord.

2.2.1 Frozen-loads optimisation: The ‘frozen-loads’ process used here is as described in Scott *et al.* [9]. The blade planform is fixed to that of the baseline and design variables (DVs) describing only the internal structure—defined in Table 2—are optimised. The objective is to minimise an augmented mass metric that accounts for the added cost of carbon [9]. Optimisation constraints include strength, buckling, fatigue, aeroelastic stability, tower clearance, and ply taper rates, as described in [9], [15]. Additions in this work include a finite strip buckling constraint [16] and a root bolt constraint. Load envelopes are computed as in Section 2.1.

2.2.2 Aero-structural optimisation: The aero-structural optimisation process uses a monolithic architecture to minimise LCoE, using the INNWIND cost model [17]. The architecture performs 600 s DLC simulations and assesses a comprehensive set of constraints at every design evaluation. This architecture enables the optimiser full control over all aeroelastic effects and allows for innovative design features to emerge from the design process. Due to space constraints, the reader is referred to the first author’s (S. Scott) thesis for full details [15]. DVs for this process are listed in Table 2, and constraints are the same as for the frozen-loads process with the addition of a tip speed constraint ($< 95 \text{ ms}^{-2}$) to limit noise and erosion.

2.3 FE modelling

To assess the blade designs, shell FE models are generated using ORE Catapult’s in-house meshing tool—BladeMesher—which reads the WindIO yaml file from ATOM, and creates an ANSYS APDL input deck. The elements used are SHELL281, 8-node quadratic. Note that elliptical cut-outs at the web run-outs are included to avoid stress concentrations.

Loads are applied as shear forces to 100 artificial nodes equally spaced along the blade reference line, which are tied to the blade spar caps using RBE3 elements. Accordingly, for each of the 12 resolved load directions, a shear force distribution is generated from the load envelopes using a least-squares method which aims to minimise the difference between the current and target internal moment distributions. Fully-fixed constraints are applied at the root nodes.

Linear static and eigen-buckling analyses are performed on the resulting FE models, in order to offer an equal comparison between the baseline and optimised designs; note that non-linear analyses would be preferable but do not converge for the baseline blade. Furthermore, pre-stress effects are included to enable the eigen-buckling analysis. Future work aims to assess buckling

Table 2: List of design variables. # DVs in brackets indicates the frozen-loads process.

Name	# DVs	Normalised location of spline control points along the blade arc-length. 0: Root - 1: Tip	Comments
<i>Aero</i>			
Blade radius	1	NA	-
Chord	6	[0 0.25 0.4 0.7 0.9 0.98]	Root/tip fixed
Thick.-to-chord	5	[0.1 0.33 0.567 0.8 1]	Root/tip fixed
Twist	6	[0 0.25 0.45 0.7 0.95 1]	-
Pitch axis	3	[0.2 0.5 1]	Dist. ref. axis to LE
Prebend	3	[0.35 0.6 1]	Root fixed
Cone angle	1	NA	-
Tilt angle	1	NA	-
<i>Structural</i>			
Shell skin	10	[0 0.02 0.05 0.1 0.25 0.4 0.6 0.8 0.9 0.95]	Glass BIAX
Root reinf.	10	[0 0.02 0.05 0.1 0.25 0.4 0.6 0.8 0.9 0.95]	Glass UD
LE reinf.	5	[0.1 0.25 0.4 0.6 0.8]	Glass UD
TE reinf.	5	[0.1 0.25 0.4 0.6 0.8]	Glass UD
Spar cap glass	8	[0.05 0.1 0.25 0.4 0.6 0.8 0.9 0.95]	Glass UD
Spar cap carbon	16	[0.05 0.1 0.25 0.4 0.6 0.8 0.9 0.95]	Carbon UD
LE core	7 (14)	[0.1 0.25 0.4 0.6 0.8 0.9 0.95]	Foam
TE core	7 (14)	[0.1 0.25 0.4 0.6 0.8 0.9 0.95]	Foam
Web 1 & 2 skin	8	[0.04 0.1 0.25 0.4 0.6 0.8 0.9 0.96]	Glass BIAX
Web 1 & 2 core	8	[0.04 0.1 0.25 0.4 0.6 0.8 0.9 0.96]	Foam
Spar cap geom.	8	[0 0.98]	
Root bolt diam.	1	[0]	
<i>Control</i>			
Tip-speed ratio	1	NA	Region II
Total	120 (107)		

using non-linear simulations so that the lowest possible partial safety factors can be used.

Lastly, strength is assessed using the Puck criterion [18], for which an in-house APDL implementation has been developed, to ensure consistency with the original criterion.

3 Analysis of the baseline

Analyses of the baseline turbine consist of aero-servo-elastic simulations to obtain a load envelope, followed by FE simulations to assess strength and buckling failures. As mentioned, the authors of the baseline recommend a structural damping of 3% which is significantly higher than those found experimentally for large blades (≈ 0.5 -1.1% [19]). In this work, it was found that a damping ratio of 6% was required for stable simulations when using the modal beam with 15 modes. However, a few trial simulations using ATOM's non-linear beam model [20] appeared to be stable with a damping ratio of 0.5%. Thus, a question mark remains over the stability analysis of large blades and more accurate methods of assessing stability are required.

Load envelopes are displayed in Figure 1, indicating the magnitude and relative contributions from each load case. The load envelopes are then applied to the FE model as described in the previous section, with strength failure indices (FIs) shown in Figure 2 for the flapMAX load case (note contours are clipped at 2 for clarity). In general, there are some small compressive fibre failures (FF) on the suction-side (SS) spar cap, whilst the pressure-side (PS) spar cap is relatively underutilised—likely due to the forced equality in the spar cap DVs. However, inter-fibre failures (IFF) for this blade are significant (greater than 10 in some localised spots), and failures can be found in the skins, webs, and LE/TE reinforcement. The significant IFFs can be

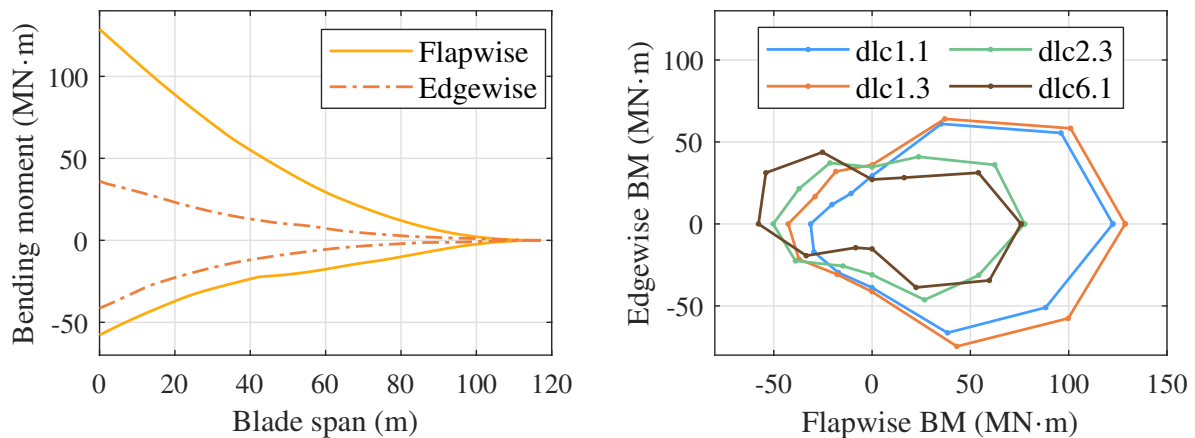


Figure 1: Blade spanwise, and root clock-face, load envelopes for the baseline. Loads quoted in the element coordinate system, safety factors included.

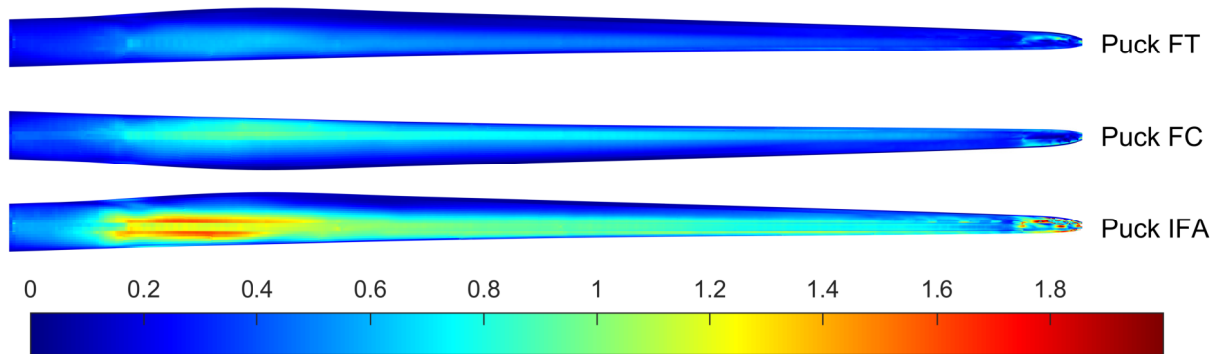


Figure 2: Strength failure indices for the baseline—flapMAX load case. Contours clipped at 2. FT = fibre tension, FC = fibre compression, IFA = inter-fibre mode A.

attributed to the fact that WISDEM currently only performs a low-fidelity check on longitudinal strains, and omits any transverse, shear, or inter-fibre checks. Furthermore, the baseline blade exhibits extremely low buckling resistance as stated in Table 4 (for some load cases less than 3% of the design loads). Critical buckling failures near the tip are likely due to low spar cap thickness, and elsewhere on the blade due to insufficient core material in the panels. Lastly, the tower clearance constraint is satisfied but far from optimal, and fatigue failures (as computed in ATOM) are significant. These failures motivate the optimisations conducted in this work.

4 Optimisation results

Global metrics for the optimised designs are shown in Table 3. It is noted that due to space constraints, discussion is limited to global metrics and key features in the resulting designs. The reader is referred to [15] for exhaustive discussion on auxiliary topics such as gradients (Chapter 4), convergence (Chapter 7), and detailed analysis of bend-twist coupling solutions (Chapters 6 and 8); albeit for a 20 MW system.

It can be seen that the frozen-loads design displays an increase in LCoE due to the higher blade mass. As demonstrated in Section 3, the planform of the baseline design produces high loads relative to the structures ability to withstand those loads. Therefore, fixing the planform and only designing an internal structure inherently requires more material to ensure feasibility. In contrast, the aero-structural optimised design offers a significant LCoE reduction,

Table 3: Comparison of design metrics. All % differences are relative to baseline.

Metric	Baseline	Frozen-loads		Aero-struct	
		Val.	%	Val.	%
LCoE (€/MWh)	93.32	94.19	0.93%	91.19	-2.29%
AEP (GWh)	78.29	78.24	-0.07%	79.47	1.49%
Blade mass (tn)	71.08	95.72	34.7%	63.05	-11.3%
Specific power (W/m ²)	329	329	0%	304	-7.67%
Capacity factor (%)	0.596	0.596	-0.06%	0.605	1.49%
Blade arc length (m)	117.15	117.15	0%	122.23	4.34%
Solidity (%)	3.14	3.14	0%	3.24	3.48%
Cone (°)	4	4	0%	4.56	13.9%
Tilt (°)	6	6	0%	2.4	-60.3%
Tip prebend (m)	-4	-4	0%	-4.81	20.29%
Rated wind speed (m/s)	10.67	10.69	0.16%	10.56	-1%
Max. tip speed (m/s)	91.47	90.71	-0.83%	94.68	3.51%
TSR (-)	8.56	8.48	-0.99%	8.97	4.77%
1 st blade freq.	0.488	0.333	-31.6%	0.449	-8.09%
2 nd blade freq.	0.689	0.555	-19.5%	0.673	-2.31%

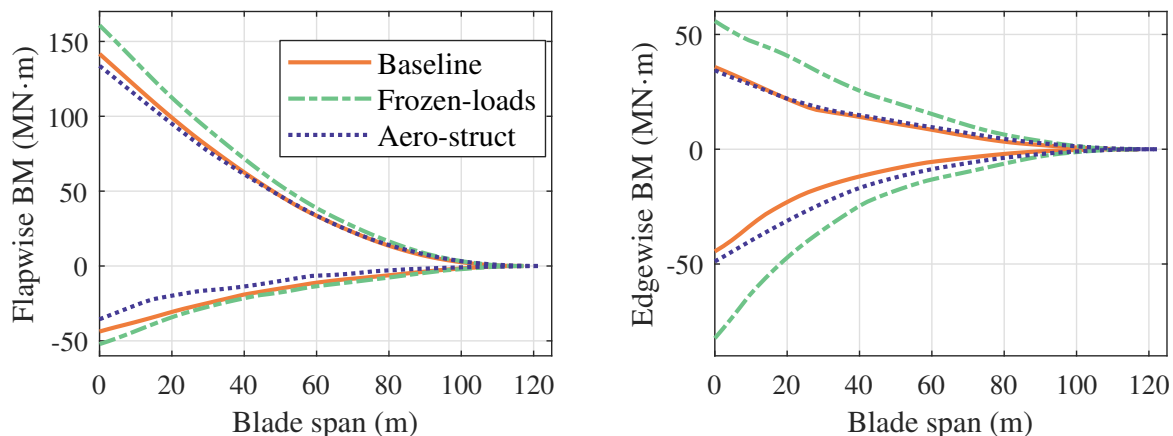


Figure 3: Spanwise load envelopes for the baseline and optimised blades. From piecewise linear simulations and reduced set of DLCs.

due to improvements in energy yield and reductions in blade mass. Optimising LCoE entails a balancing act between maximising AEP and minimising costs—these typically being in opposition. However, using a monolithic architecture as done here allows for the AEP-cost balance to be finely tuned, and even for features such as passive load alleviation to ‘ease’ the balance by enabling more power for the same loads (and cost), or vice-versa.

Relative to the baseline, the aero-structurally optimised blade is 4.3% longer yet offers a small reduction in ultimate loads (see Figure 3). Accordingly, greater section thickness and chord near the root (see Figure 4) are employed to add stiffness, hence more efficiently satisfying the failure constraints. The aforementioned load reductions are the result of a smaller chord near the tip, less aerodynamic aerofoils, and a strong nose-down bend-twist response ($\approx 7^\circ$ at rated). This bend-twist response can be explained using Figure 5, in which a simple blade planform is plotted, including the spar cap locations, flexural axis (FA) (computed as in [21]), aerodynamic centre (AC), and mass centre. The optimiser’s choice to move the spar caps (and hence the FA) toward the LE, as well as for a short distance between LE and the straight pitching axis, results

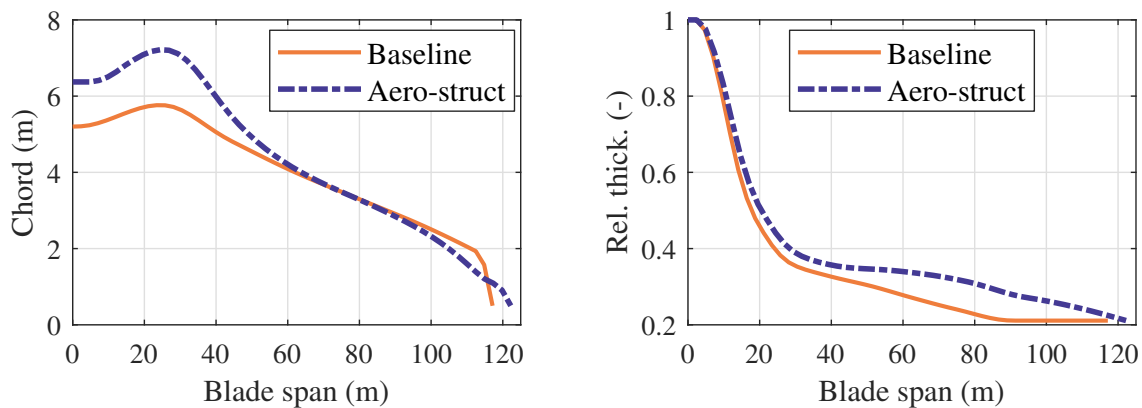


Figure 4: Chord and relative thickness distributions.

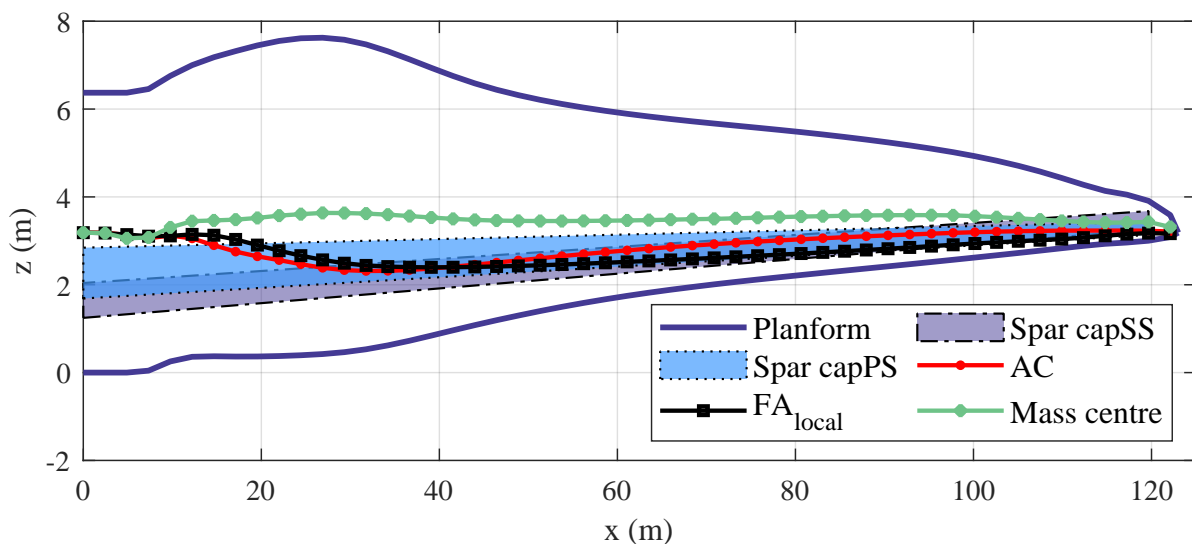


Figure 5: Planform showing aerodynamic centre, flexural axis, mass centre and spar cap locations.

in the AC being rearward of the FA. Thus, a nose-down twisting moment is generated upon any downwind flapwise aerodynamic force. Importantly, this bend-twist response is induced without the use of sweep or fibre steering, i.e. the methods most commonly applied in recent literature, as these come with associated drawbacks such as increased torsional loads, reductions in stiffness, and manufacturing/transport difficulties [22]. Note the kink in the planforms LE near the root is due to the optimiser sharply varying the pitch axis DV outboard from the enforced region of root tangency. Whilst the kink is far smoother when plotted with equal x - y axis scaling, a smoothness constraint or minor tweaking of the DV locations would avoid this. Furthermore, centrifugal forces are included in the simulations so the optimiser considers straightening effects.

5 FE shell analysis of optimised blades

This section now presents the results, and insights gained, from FE shell modelling of the optimised blades. Strength FIs for the frozen-loads and aero-structural optimised blades are plotted in Figures 6 and 7, respectively, for the flapMAX load case. In addition, the maximum FIs from all load cases are plotted with respect to the blade span in Figure 8. As can be seen,

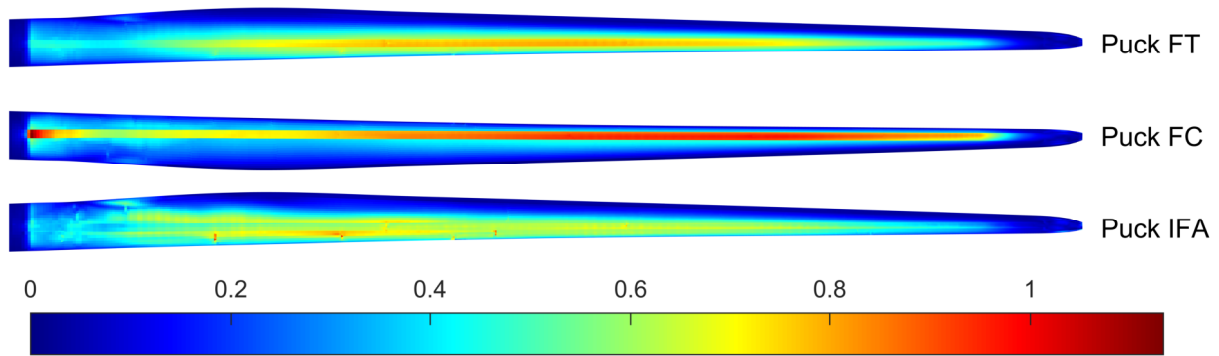


Figure 6: Contour plot of failure indices for the frozen-loads blade for maximum flapwise load case

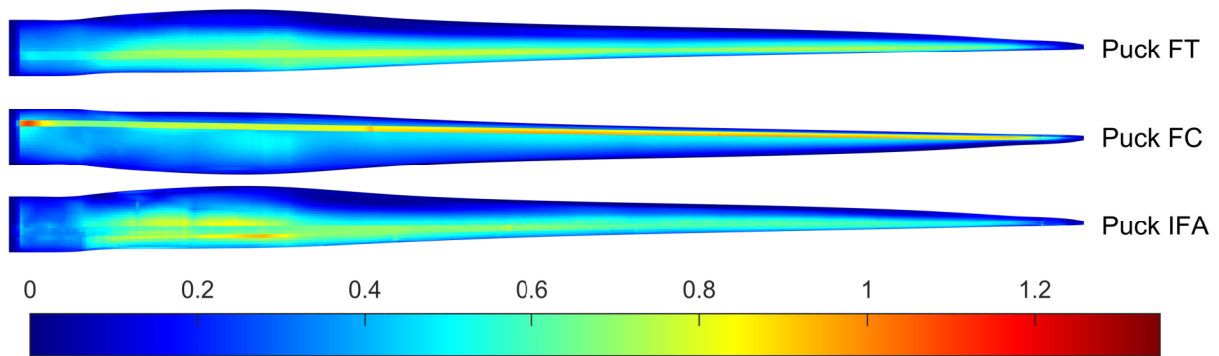


Figure 7: Contour plot of failure indices for the aero-structural blade for maximum flapwise load case

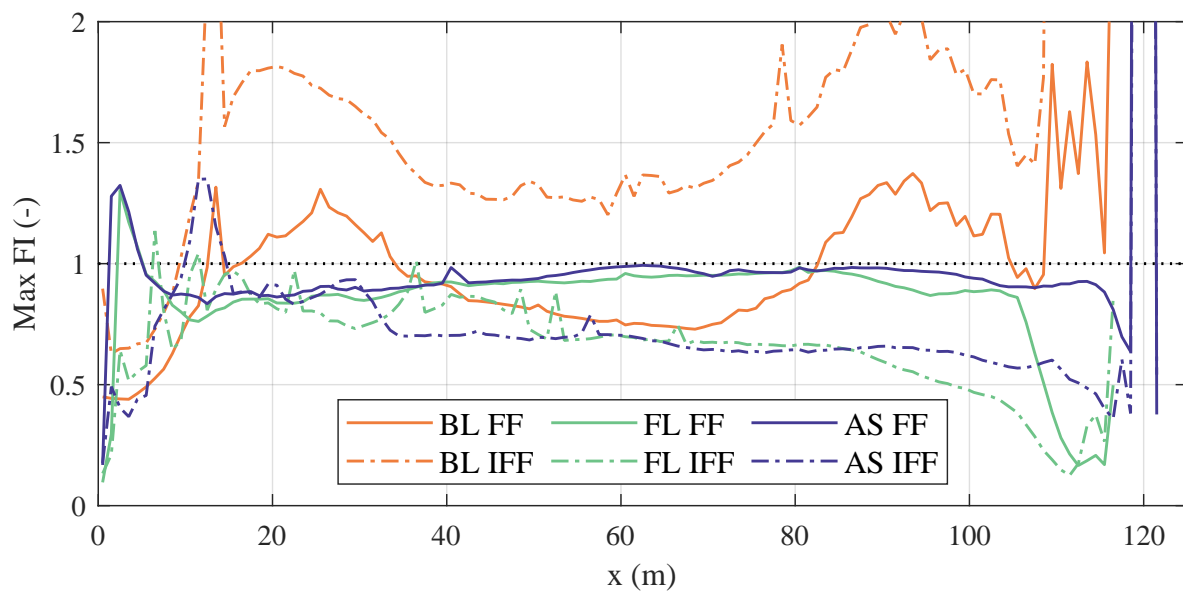


Figure 8: Comparison of maximum FIs. BL = baseline, FL = frozen-loads, AS = aero-struct.

both designs resolve the strength failure issues found with the baseline, albeit for the frozen-loads design feasibility comes at the expense of increased blade mass.

For both models, a major strength driver is fibre compression on the SS spar cap. It can be seen that both blades have FI close to 1 for much of the spar cap, indicating this key structural

Table 4: Location of critical buckling mode and buckling RFs for the three blades.

	1 (flapMAX)		4 (edgeMAX)		7 (flapMIN)		10 (edgeMIN)	
	Loc. (m)	RF	Loc. (m)	RF	Loc. (m)	RF	Loc. (m)	RF
Baseline	110	0.03	103	0.04	112	0.03	115	0.47
Frozen-loads	11.3	1.21	12.7	1.39	78.8	1.08	7.7	1.43
Aero-struct	7.13	0.74	7.51	1.03	7.51	1.01	31.8	1.07

element is both well-utilised and adequately predicted by the lower fidelity model. This is confirmed by the maximum FF indices in Figure 8. The PS spar caps are less utilised from a strength perspective (FIs ≈ 0.8 for fibre tension) due to the higher tensile strength of carbon and the typically smaller upwind flapwise loads. Thus, the PS caps are more stiffness driven. IFF is predominantly design driving on the PS of the blades, with IFF mode A (matrix tension + shear) being the most critical as the matrix is weakest in tension. The most design driving region for IFF is along the region boundaries between spar cap and sandwich panels. Given the low-fidelity representation of the blade used in ATOM, there is a simple step change in thickness at this boundary, as opposed to a thickness taper, or, as might be found in a real blade, staggered ply drops and tapered core material. Thus, stress concentrations arise along this boundary which could likely be mitigated to some extent by a higher fidelity representation.

Table 4 defines the locations and buckling load factors for the critical buckling mode, for each of the four main load directions. Whilst the buckling resistance of the optimised designs significantly improves on the baseline, these values would not be acceptable in practice for not meeting the target load factor (RF) of 1.62 (note 1.62 includes reduction factors according to [23]). Results indicate that the lower fidelity buckling checks in ATOM are not conservative, which is unsurprising given the known limitations of panel methods and the finite-strip method when applied to a full wind turbine blade. Improving buckling predictions within an optimisation context is an active area of research for both the University of Bristol and ORE Catapult.

Overall, strength FIs in the main load-bearing components are predicted well by ATOM, especially when considering the significant reduction in computational effort compared to a shell model. This work indicates that the areas typically predicted poorly are localised stress concentrations, such as web terminations, or step changes in material at region boundaries. It is likely, however, that the required modifications to achieve feasibility in the higher fidelity model, and crucially the resulting difference in aeroelastic properties, would be minimal. This is an important point for preliminary system-design tools, as whilst they can produce innovative aeroelastic synergies, it is crucial that such properties be retained when moving to more detailed design phases.

6 Conclusions

This work employs two optimisation processes to develop a structurally and dynamically feasible blade design for the IEA 15 MW wind turbine. There remains a question mark over the baseline blades aeroelastic stability, given the unrealistically high value of structural damping required for some simulation methods. Furthermore, inter-fibre strength, buckling, and fatigue failures are significant; whilst the spar caps exhibit only minimal fibre failures.

Given these shortcomings, the first design presented uses a frozen-loads internal structure optimisation—with fixed planform—to minimise blade mass. The second applies a monolithic aero-structural architecture to minimise LCoE with aerodynamic, structural, and control DVs. The frozen-loads design results in an LCoE increase of 0.93% due to the mass penalty of satisfying the feasibility constraints. In contrast, the aero-structural design offers an LCoE reduction of 2.29% due to improved AEP and reduced blade mass. Subsequent FE shell analyses of the optimal blades indicate that strength failures are well predicted and the structural material

well utilised by the optimiser. However, buckling load factors do not satisfy the required target values, indicating the low-fidelity buckling checks in ATOM are not conservative.

Acknowledgments

The authors would like to thank the Wind Blades Research Hub (WBRH), a collaboration between the University of Bristol and ORE Catapult, for their support of this work.

Data statement

The resulting designs are publicly available in the format specified by the [WindIO](#) yaml ontology. The link to the yaml files can be found on the [IEA 15 MW GitHub](#) repository or on the University of Bristol research data [storage](#) under the name "IEA15MW_Bristol".

References

- [1] J. Jonkman, S. Butterfield, *et al.*, "Definition of a 5-MW Reference Wind Turbine for Offshore System Development," NREL, Colorado, Tech. Rep. February, 2009.
- [2] C. Bak, F. Zahle, *et al.*, "Description of the DTU 10 MW Reference Wind Turbine Department of Wind Energy I-Report," no. July, pp. 1–138, 2013.
- [3] P. Bortolotti, H. Canet Tarrés, *et al.*, "Systems Engineering in Wind Energy - WP2.1 Reference Wind Turbines," *IEA Wind TCP Task 37*, no. May, 2019.
- [4] E. Gaertner, J. Rinker, *et al.*, "IEA Wind TCP Task 37: Definition of the IEA 15-Megawatt Offshore Reference Wind Turbine," pp. 1–44, 2020.
- [5] K. Dykes, P. Graf, *et al.*, "Introducing WISDEM: An Integrated System Modeling for Wind Turbines and Plant," in *Third Wind Energy Systems Engineering Workshop*, Boulder, 2015.
- [6] J. Rinker, E. Gaertner, *et al.*, "Comparison of loads from HAWC2 and OpenFAST for the IEA Wind 15 MW Reference Wind Turbine," *Journal of Physics: Conference Series*, vol. 1618, no. 5, 2020.
- [7] C. L. Bottasso, P. Bortolotti, *et al.*, "Integrated aero-structural optimization of wind turbines," *Multibody System Dynamics*, vol. 38, no. 4, pp. 317–344, 2016.
- [8] P. Bortolotti, A. Kapila, *et al.*, "Comparison between upwind and downwind designs of a 10 MW wind turbine rotor," *Wind Energy Science*, vol. 4, no. 1, pp. 115–125, 2019.
- [9] S. Scott, P. Greaves, *et al.*, "Efficient structural optimisation of a 20 MW wind turbine blade," in *Journal of Physics: Conference Series*, 2020.
- [10] T. Macquart, V. Maes, *et al.*, "A New Optimisation Framework for Investigating Wind Turbine Blade Designs," in *12th World Congress of Structural and Multidisciplinary Optimization*, ISSMO, 2017.
- [11] S. Scott, T. Macquart, *et al.*, "Preliminary validation of ATOM: an aero-servo-elastic design tool for next generation wind turbines," *Journal of Physics: Conference Series*, vol. 1222, 2019.
- [12] NREL, "ROSCO. Version 2.3.0," *GitHub Repository*, 2021. [Online]. Available: <https://github.com/NREL/rosco>.
- [13] International Electrotechnical Commission, *BS EN IEC 61400-1:2019 Wind energy generation systems - Part 1: Design requirements*. BSI Standards Limited, 2019, ISBN: 978 0 539 06623 4.
- [14] T. Macquart, S. Scott, *et al.*, "Piecewise linear aeroelastic rotor-tower models for efficient wind turbine simulations," *Journal of Physics: Conference Series*, vol. 1618, p. 042 033, 2020, ISSN: 1742-6588.
- [15] S. J. Scott, "Optimal Aeroelastic Tailoring of Wind Turbines," Ph.D. dissertation, 2021.
- [16] B. Schafer, *CUFISM - Cross-section elastic buckling analysis v5.04*, 2019. [Online]. Available: <https://www.ce.jhu.edu/cufism/>.
- [17] P. Chaviaropoulos, F. Rasmussen, *et al.*, "PI-based assessment (application) on the results of WP2-WP4 for 20 MW wind turbines," *INNWIND Deliverables*, no. September, 2017.
- [18] A. Puck and H. Schürmann, "Failure analysis of FRP laminates by means of physically based phenomenological models," *Composites Part B: Engineering*, vol. 58, pp. 1045–1067, 1998.
- [19] D. I. Chortis, N. A. Chrysochoidis, *et al.*, "Damped structural dynamics models of large wind-turbine blades including material and structural damping," *Journal of Physics: Conference Series*, 2007.
- [20] T. Macquart, S. Scott, *et al.*, "Corotational Finite Element Formulation for Static Nonlinear Analyses with Enriched Beam Elements," *AIAA Journal*, pp. 1–17, 2020, ISSN: 0001-1452.
- [21] O. Stodieck, J. E. Cooper, *et al.*, "Interpretation of bending/torsion coupling for swept, nonhomogenous wings," *Journal of Aircraft*, vol. 53, no. 4, pp. 892–899, 2016, ISSN: 15333868.
- [22] S. Scott, M. Capuzzi, *et al.*, "Effects of aeroelastic tailoring on performance characteristics of wind turbine systems," *Renewable Energy*, vol. 114, pp. 887–903, 2017, ISSN: 18790682.
- [23] DNV-GL, *DNVGL-ST-0376 Rotor blades for wind turbines*, 2015.